IOP Publishing Journal of Optics

J. Opt. **12** (2010) 104015 (9pp) doi:10.1088/2040-8978/12/10/104015

# Light pulse manipulation in $Sn_2P_2S_6$

**A Shumelyuk and S Odoulov**

Institute of Physics, National Academy of Sciences, 46, Science Avenue, 03 650 Kyiv, Ukraine

E-mail: shumeluk@iop.kiev.ua

Received 8 February 2010, accepted for publication 16 March 2010
Published 24 September 2010
Online at stacks.iop.org/JOpt/12/104015

**Abstract**
Acceleration and deceleration of light pulses when writing a refractive index grating in $Sn_2P_2S_6$ is described. It is shown that in crystals with two types of movable charge carriers short pulses are accelerated while long pulses are delayed or vice versa, depending on the orientation of the polar axis.

**Keywords:** light slowing down, photorefractive gratings, crystals with bipolar conductivity

## 1. Introduction

To slow down or to accelerate a pulse of light one needs to find an appropriate system that features strong enough optical dispersion and can therefore affect the group velocity of light [1]. The necessary dispersion may occur near the optical resonances of atoms or molecules in gases [1], those of the impurities or collective excitations in solid states [2], etc. The other useful type of resonances has a spatial origin, it occurs in inhomogeneous media with the size of structural elements comparable to the light wavelength. These may be, for example, arrays of micro-cavities [3] or 3D optical gratings with Bragg resonances [4].

The resonances in question can exist in a homogeneous medium or specially designed inhomogeneous sample even with no light illuminating them (linear systems). They can also be created by light, especially by light pulses that are intended to be decelerated or accelerated. These are essentially nonlinear systems based, for example, on electromagnetically induced transparency [5], quantum coherence resonance in homogeneously broadened lines [6], or light induced transient gratings of the refraction index [7–9].

Bragg resonances of index gratings in photorefractives are extremely narrow because of the slow nonlinear response defined by the dielectric relaxation time of these crystals. The HWHM of their gain spectra can go far below 1 Hz, resulting in a group velocity of decelerated pulses of the order of $10^{-2}$ cm $s^{-1}$ [7].

Dynamic-grating-induced pulse deceleration does not require a precise adjustment of the light wave frequency(ies) to certain resonance(s): it can be achieved within a fairly wide spectral range in which the relevant optical nonlinearity ($\chi^{(3)}$ or photorefractive) is sufficiently strong. The low power light pulses from conventional gas lasers (He–Ne, $Ar^+$) can be decelerated at ambient temperature. These are the obvious advantages of the grating technique as compared to other nonlinear techniques. There are however also important limitations. Mostly they are similar to those of other known techniques: for example, the best fractional delay time achieved at present is close to one; also, the severe problem of limited bandwidth is unsolved [10]. Among the possible practical uses of photorefractive grating pulse manipulations is their application in white-light interferometers for detection of gravitational waves [11]. The quite slow response of photorefractive crystals made possible the detailed investigation of fundamental properties of the optical forerunners associated with Bragg grating resonances [12].

Since the first reports on pulse deceleration with photorefractive crystals were published in 2003 [7, 8], several important contributions have been made, both in experiment and in calculation. Pulse deceleration and acceleration was reported in crystals of the sillenite family with applied electric field [9, 13]. The pulse acceleration was achieved with no external field, when mixing two counterpropagating waves in SBN:60 [14]. The necessary anomalous dispersion was ensured by the gain doublet that appeared when mixing a signal with two symmetrically shifted components in the pump wave. The pulse deceleration in photorefractives with local nonlinear response was theoretically analysed in [15]. Finally, backward wave four wave mixing was suggested in [16] as a suitable process for pulse manipulation.

The present article is devoted to pulse manipulations (deceleration and acceleration) in tin hypothiodiphosphate ($Sn_2P_2S_6$, SPS). This material ensures quite large coupling strength in red and near infrared domains of the spectrum [17, 18] and is efficient up to communication wavelength 1.5 $\mu$m [19]. In addition, it shows photoconductivity which

 

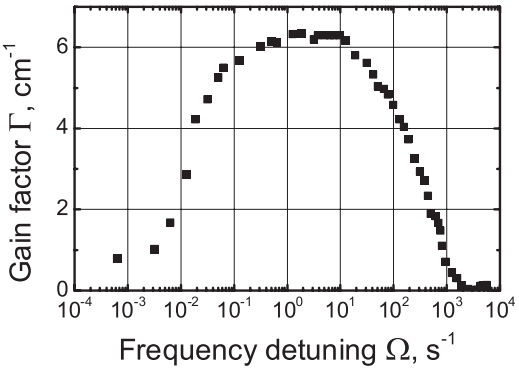


**Figure 1.** Dependence of two-beam coupling gain factor Γ in SPS on frequency detuning of the signal wave with respect to the pump wave for $\lambda = 633$ nm and $K = 2.2\ \mu\text{m}^{-1}$.

is unexpectedly high for wide band gap ferroelectrics and provides therefore quite rapid nonlinear response, in the millisecond range. The undoped material [17] (and some crystals with impurities, like SPS:Se, SPS:Bi [20], SPS:Sb [21]) shows two out-of-phase gratings formed by movable charge carriers of different sign [17]. After the beginning of exposure to two coherent light waves, first a 'fast' grating is recorded in the crystal by the photo-excited carriers. With the passage of time, the optically inactive carriers of different sign start to move, tending to compensate for the initial space charge grating. Such a compensation reduces, partially or completely, the transient intensity coupling, that is well pronounced at the beginning of the exposure. This unusual dynamics corresponds to an intensity gain spectrum with a narrow dip at the pump frequency and complicated dispersion spectrum [22].

Tin hypothiodiphosphate has already been used for light pulse deceleration [7, 23]. It allowed us, in particular, to prove the primary importance for slowing down of the light pulses of a high dispersion inherent to dynamic index gratings in photorefractive crystals [23]. The long duration of input pulses was chosen in these experiments to achieve saturation when two out-of-phase gratings compensate each other and the intensity coupling nearly does not exist.

The purpose of this paper is to show how this material can be used to get the light pulse acceleration exactly in the same geometry of interaction that ensures pulse deceleration, by changing only the pulse duration. To minimize the distortions of the delayed/accelerated pulse the use of matched signal and pump pulses is proposed.

## 2. Motivation

The presence of two types of movable charge carriers with considerably different dielectric relaxation times in some SPS crystals results in a complicated dependence of two-beam coupling gain factor Γ on signal detuning frequency Ω [22, 23]. A typical spectrum of $\Gamma = \Gamma(\Omega)$ measured at total light intensity $I_0 = 3\ \text{W cm}^{-2}$ when writing a transmission grating with spatial frequency $K = 2.2\ \mu\text{m}^{-1}$ is shown in figure 1.

As follows from this figure, there will be nearly no amplification of the long pulses with the spectral content $\Delta\Omega_s \leqslant 0.01\ \text{s}^{-1}$, while short pulses, with $\Delta\Omega_s \geqslant 0.1\ \text{s}^{-1}$, will be strongly amplified. The reason for this difference is in formation of the two out-of-phase photorefractive gratings with considerably different response times, 'fast' and 'slow' gratings. The short pulses propagate through the sample with only one, 'fast' photorefractive grating, while for long pulses this grating is already partially or completely compensated because of development of a 'slow' grating [18].

One can expect that a dispersion that the optical pulse feels depends on its duration $t_0$, which is the half width of the intensity profile at $1/e^2$ of the peak value for the pulse with Gaussian profile. The above statement is illustrated with figure 2, taking as an example a crystal with parameters close to those used in the experiment: slow and fast characteristic times $\tau_s = 26$ s, $\tau_f = 10$ ms, respectively, maximum coupling strength which is due to the fast grating only is $\Gamma d = 5$, 80% compensation of the initial fast grating by the slow grating in the steady state, where Γ is the intensity gain factor and $d$ is a sample thickness. For pulses that are much shorter than the slow characteristic time of the crystal $t_0 \leqslant \tau_s$, the spectra of gain factor and dispersion must not differ much from those typical for crystals with unipolar conductivity (figures 2(a) and (b)). The spectral content of a 0.015 s pulse fits to the domain of the dispersion spectrum with a negative slope and therefore such a pulse must be decelerated.

Surprisingly, even for such a short pulse with $t_0 \approx 0.001\tau_s$ the shallow dip in the gain profile is already seen and the dispersion spectrum features a narrow flat shoulder, with the slope tending to zero. This can be seen in figures 2(c) and (d), which show a zoomed area of figures 2(a) and (b) in the vicinity of $\Omega = 0$. These singularities are, however, too weak to affect considerably the shape of the delayed pulse.

With the increasing pulse duration the amplitude of the compensating grating grows, the dip in gain spectrum becomes larger and the slope of the dispersion near $\Omega = 0$ changes sign. This should result in splitting of the output pulse into two parts, one delayed and the other advanced compared to the input pulse. Finally, for quite long pulses, $t_0 \approx 4\tau_s$, the gain spectrum and dispersion spectrum are close to saturation (figures 2(e) and(f)) and the total spectral content of the pulse now fits to a narrow range of the dispersion curve with positive slope. Thus, such a pulse should be accelerated with no considerable distortion.

We check these qualitative considerations experimentally with $Sn_2P_2S_6$ crystals and by numerical simulation, as described in the following sections.

## 3. Experiment

The experiments are performed with SPS crystals grown in the Institute of Solid State Physics and Chemistry, Uzhgorod State University, Uzhgorod, Ukraine. The samples are selected that feature a pronounced electron–hole competition in formation of the space charge grating (nominally undoped crystals of type 1 [18]). Typical sample dimensions are $9 \times 4.5 \times 9\ \text{mm}^3$ along $x$-, $y$-, and $z$-axes. They ensure a strong transient gain (of the order of several hundred-fold) for a weak signal beam, followed by a slow decrease to the much smaller gain value

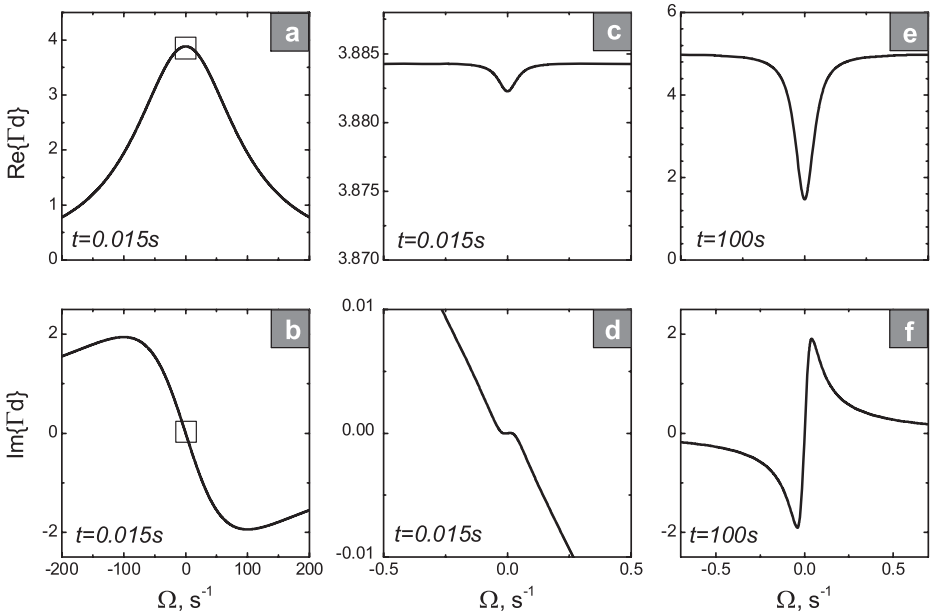


**Figure 2.** Spectra of the real and imaginary parts of the coupling strength in SPS for different exposure times, $t = 0.015$ s for (a)–(d), and $t = 100$ s for (e) and (f). (c), (d) Zoomed areas within the small squares in (a) and (b).

(of the order of a fewfold) with light beams from conventional He–Ne laser of 50 mW output intensity [18]. The characteristic times of gain build-up $\tau_f$ and compensation $\tau_s$ are in ranges of tens of milliseconds and tens of seconds, respectively, for total light intensity in the sample $I_0$ up to 3 W cm$^{-2}$ and grating spatial frequency $K \simeq 3.5\ \mu$m$^{-1}$.

Two horizontally polarized light beams impinge upon the sample through the $z$-face so that the photorefractive grating vector **K** is parallel to the $x$-axis (figure 3). This exploitation of geometry allows the largest electrooptic coefficient of SPS $r_{11}$ [24] and optimizes the gain factor for copropagating waves. The electrooptic modulator EOM is put in front of the photorefractive crystal PRC in the signal wave. The signal generator SG and amplifier (not shown in figure 3) produce an electric pulse of Gaussian profile for the electrooptic modulator. In such a way a light pulse with a controllable pulse duration is formed in the signal beam. There are several reasons to chose the Gaussian temporal envelope. Compared to the Lorentzian shape it has more quickly decreasing tails, i.e., the pulse is more sharp. Compared to the rectangular pulse it has a less extended spectrum, so that for any given bandwidth the shape of the delayed Gaussian pulse can be reproduced with better fidelity than the shape of the rectangular pulse of the same duration. Last but not least, Gaussian shape is also more suitable for calculations. The intensities of the input and output beams are measured with photo-detectors $D_1$ and $D_2$.

Figure 4 shows typical temporal envelopes of input and output pulses for the input pulse duration $t_0 = 150$ ms, 0.54 s, 1 s, 11. 8 s, and 200 s for frames (a), (b), (c), (d) and (e), respectively, for the case when the signal wave is amplified. For short input pulses with $\tau_s \leqslant t_0 \leqslant \tau_f$ the output pulse is delayed (figure 4(a)). With the increasing $t_0$, however, the delay becomes smaller (figure 4(b)) and changes sign: the output pulse appears to be advanced with

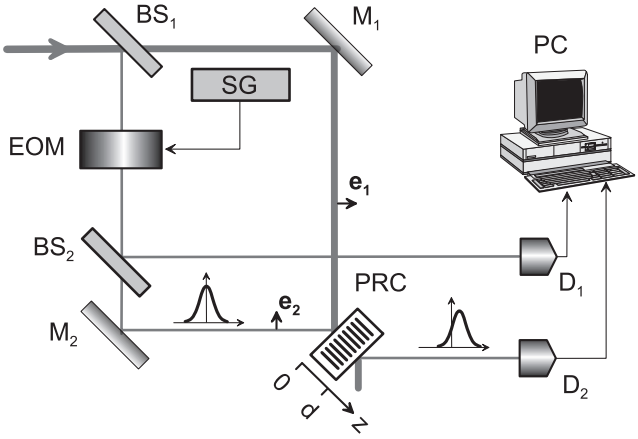


**Figure 3.** Schematic diagram of the experimental setup. Two coherent light waves impinge upon photorefractive crystal PRC, the shape of the signal pulse is controlled by electrooptic modulator EOM driven by signal generator SG. The detectors $D_1$ and $D_2$ monitor the temporal variations of the input and output pulses; their signals are stored with the PC-based data acquisition system. $M_i$ are the mirrors and $BS_i$ are the beamsplitters. The unit vectors $e_1$ and $e_2$ show polarization of interacting waves.

respect to the input. This acceleration is clearly seen already for $t_0 = 1$ s (figure 4(c)). Simultaneously, the secondary maximum develops in the output pulse; its amplitude grows with increasing $t_0$ (figures 4(c) and (d)). For very long input pulse, $t_0 \geqslant \tau_s$, this secondary maximum disappears and the advanced pulse becomes close in shape to the input pulse (figure 4(e)).

For large exposure times two out-of-phase gratings with high amplitudes nearly compensate each other. This leads to increased sensitivity of the system to even minor phase mismatch, caused, for example, by mechanical instabilities.

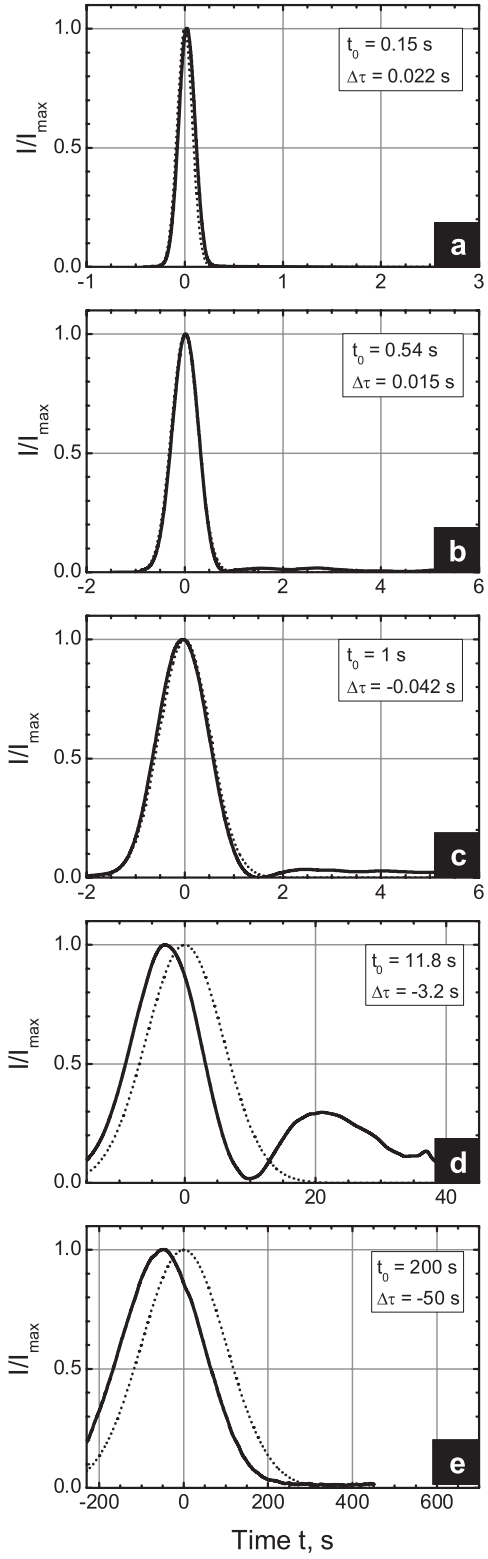


**Figure 4.** Temporal variations of the signal intensity at the input (black dots) and output (solid lines). The input pulse duration is $t_0 = 0.15$ s, 0.54 s, 1 s, 11.8 s, and 200 s for (a), (b), (c), (d), and (e), respectively; $I_0 = 3$ W cm$^{-2}$ and $K = 3.5\ \mu$m$^{-1}$.

The output pulses for $t_0 = 200$ s are therefore quite noisy. The Gaussian fit, shown in figure 4(e), clearly indicates nevertheless a considerable advancement of the output pulse with respect to the input.

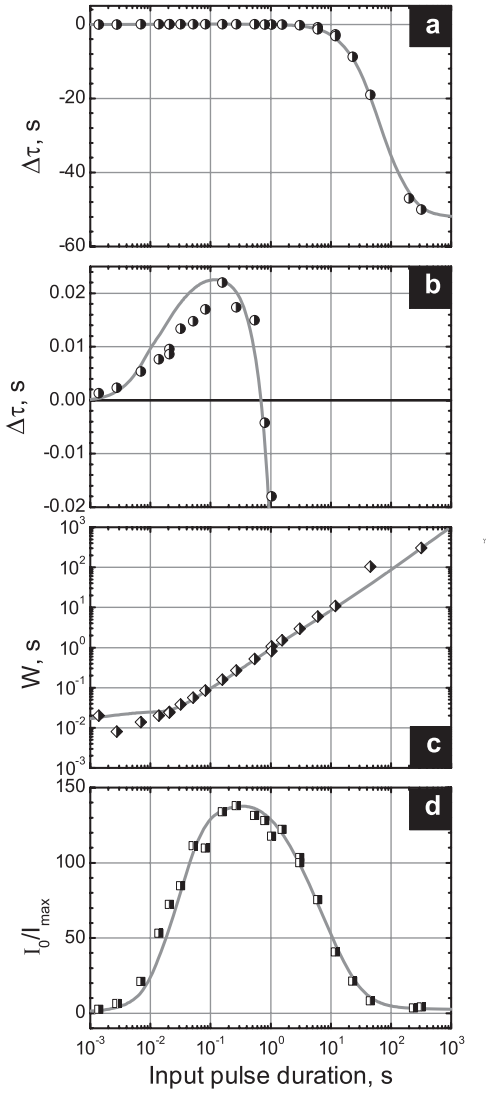


**Figure 5.** Experimentally measured pulse delay time $\Delta\tau$ ((a), (b)), pulse duration $W$ (c) and pulse amplification $I_s^{max}(d)/I_s^{max}(0)$ (d) versus input pulse duration $t_0$ are shown by filled dots. The grey solid lines represent the dependences calculated with $\tau_f = 0.01$ s, $\tau_s = 26$ s, $\Gamma_f d = 5$ and $\Gamma_s d = -0.8\Gamma_f d$, as explained in section 3.

If the polar axis of the SPS sample is rotated to 180° we observe a complimentary picture: the short input pulses become accelerated while the long input pulses start to be decelerated. This is a consequence of the non-locality of the crystal response and the spatial shift of the photorefractive grating to a quarter of its spacing in the direction of the polar axis. The 180° rotation of the crystal changes the direction of the beam intensity coupling and the sign of dispersion, thus switching from acceleration to deceleration or vice versa.

From data like those shown in figure 4 the dependences of the output pulse delay $\Delta t$, duration $W(d)$, and amplitude $I_s^{max}(d)/I_s^{max}(0)$ on the input pulse duration $t_0$ have been constructed (figure 5). In figure 4 all pulses shown are normalized to their maximum intensity. In fact, as one can see from figure 5(d), the short pulses are strongly amplified (up to 140-fold) while pulses with $t_0 = 100$ s are amplified only threefold.

## 4. Calculations of temporal profiles

To calculate the temporal envelopes of the output pulses we use the same procedure as described in paper [7], based on the traditional two-beam coupling approach. Two equations for slowly varying amplitudes of the signal and pump waves, $A_s$ and $A_p$, respectively, are

$$\frac{\partial A_s}{\partial z} = -\frac{i\pi n^3 r}{2\lambda} E_K A_p, \qquad \frac{\partial A_p}{\partial z} = -\frac{i\pi n^3 r}{2\lambda} E_K^* A_s, \quad (1)$$

with the electrooptic constant $r$ ($r_{11}$ for the considered case of SPS), index of refraction $n$, and wavelength $\lambda$.

Following [25, 26, 22, 27], the amplitude of the space charge field $E_K$ consists of two contributions $E_K = ie(N_K + H_K)/\epsilon\epsilon_0 K$ that represent the amplitudes of redistributed positive and negative charges, $N_K$ and $H_K$, respectively. The dynamics of the development for these two distributions are described by the equations

$$\frac{\partial N_K}{\partial t} + \gamma_{11} N_K + \gamma_{12} H_K = \frac{1}{2}\left(\frac{m N_{\text{eff}} K^2 R_p^2}{1 + K^2 L_D^2}\right)\left(\frac{\sigma_p}{\epsilon\epsilon_0}\right), \quad (2)$$

$$\frac{\partial H_K}{\partial t} + \gamma_{21} N_K + \gamma_{22} H_K = 0, \quad (3)$$

with the complex modulation index $m = 2A_s A_p^*/I_0$, total intensity $I_0 = |A_s|^2 + |A_p|^2$, effective trap density $N_{\text{eff}}$, spatial frequency of the grating $K$, dielectric constant $\epsilon\epsilon_0$, diffusion length $L_D$, screening lengths $R_{p,H}$, and fast component of photoconductivity $\sigma_p$ [27]. The generation term in the right-hand side of equation (2) is linearly dependent on total intensity via photoconductivity $\sigma_p = \kappa I_0$, where $\kappa$ is the specific photoconductivity. There is no generation term in the right-hand side of equation (43) because the negative charges are excited thermally.

$$\gamma_{11} = \left(\frac{\sigma_p}{\epsilon\epsilon_0}\right)\left(\frac{1 + K^2 R_p^2}{1 + K^2 L_D^2}\right),$$
$$\gamma_{22} = \left(\frac{\sigma_H}{\epsilon\epsilon_0}\right)(1 + K^2 R_H^2), \quad (4)$$
$$\gamma_{12} = \left(\frac{\sigma_p}{\epsilon\epsilon_0}\right)\left(\frac{1}{1 + K^2 L_D^2}\right), \qquad \gamma_{21} = \left(\frac{\sigma_H}{\epsilon\epsilon_0}\right).$$

They define the two characteristic relaxation times, slow ($\tau_s$) and fast ($\tau_f$),

$$\tau_{f,s} = \frac{2}{\gamma_{11} + \gamma_{22} \pm \sqrt{(\gamma_{11} - \gamma_{22})^2 + 4\gamma_{12}\gamma_{21}}}. \quad (5)$$

For SPS, with its strong difference of dielectric relaxation times $\tau_{di}^{(p)} \leqslant \tau_{di}^{(H)}$ the fast time roughly coincides with the characteristic time of fast grating build-up, while for the slow time we have a $K^{-2}$ dependence, which is characteristic for ambipolar diffusion:

$$\tau_f \simeq \left(\frac{\epsilon\epsilon_0}{\sigma_f}\right)\left(\frac{1 + K^2 L_D^2}{1 + K^2 R_p^2}\right),$$
$$\tau_s \simeq \left(\frac{\epsilon\epsilon_0}{\sigma_s}\right)\frac{1}{K^2}\left(\frac{1 + K^2 R_p^2}{K^2 R_p^2 R_H^2 + R_p^2 + R_H^2}\right). \quad (6)$$

Equation (5) can be found in all papers [25, 22, 27] mentioned above, but a correct interpretation of the slow time as the ambipolar diffusion time was first given in [27].

We consider in what follows the cw pump wave intensity and Gaussian profile of the input signal wave amplitude with pulse duration $t_0$

$$A_s(0, t) = A_{s0} \exp(-t^2/t_0^2) \quad (7)$$

in the undepleted pump approximation, $|A_s|^2 \leqslant |A_p|^2$. To find, therefore, the temporal envelope of the output pulse, $|A_s(d, t)|^2$, it is necessary to solve three equations, (1), (3) and (4).

By moving to the frequency domain when taking the Fourier transform $A_s(z, t) \rightarrow A_s^{\omega}(z)$ it is possible to get at the output

$$A_s^{\omega}(d) = A_s^{\omega}(0) \exp(\Gamma d/2), \quad (8)$$

where the complex coupling constant $\Gamma$ reads

$$\Gamma(\Omega) = \frac{\Gamma_p}{1 - i\Omega\tau_f} + \frac{\Gamma_H}{(1 - i\Omega\tau_f)(1 - i\Omega\tau_s)} \quad (9)$$

and possesses a real Re($\Gamma$) and an imaginary Im($\Gamma$) part responsible for the intensity and phase coupling, respectively. Here $\Gamma_H$ and $\Gamma_p$ are interrelated by the equation

$$\Gamma_H = -\Gamma_p \frac{R_p^2}{K^2 R_p^2 R_H^2 + R_p^2 + R_H^2}. \quad (10)$$

Performing now an inverse Fourier transform of a function (8) with coupling coefficient (9) it is possible to get

$$A(d, t) = \frac{A_s(0, t) t_0}{\sqrt{\pi}} \int_0^{\infty} \exp\left[\frac{\Gamma_p d}{2(1 + \Omega^2\tau_f^2)} + \frac{\Gamma_H d(1 - \Omega^2\tau_f\tau_s)}{2(1 + \Omega^2\tau_f^2)(1 + \Omega^2\tau_s^2)} - \frac{\Omega^2 t_0^2}{4}\right] \times \cos\left[\frac{\Gamma_H \Omega(\tau_f + \tau_s)}{2(1 + \Omega^2\tau_f^2)(1 + \Omega^2\tau_s^2)} + \frac{\Gamma_p d\Omega\tau_f}{2(1 + \Omega^2\tau_f^2)} - \Omega t\right] d\Omega \quad (11)$$

where $t_0$ is the input pulse duration.

For very short pulses, with duration $t_0 \ll \tau_s, \tau_f$ the pulse spectrum is wide, $\Omega\tau_s \rightarrow \infty$ and equation (11) reduces to the expression

$$A(d, t) = \frac{A_s(0, t) t_0}{\sqrt{\pi}} \times \int_0^{\infty} \exp\left(-\frac{\Omega^2 t_0^2}{4} + \frac{1}{2}\frac{\Gamma_p d}{1 + \Omega^2\tau_f^2}\right) \times \cos\left(-\frac{1}{2}\frac{\Omega\tau_f \Gamma_p d}{1 + \Omega^2\tau_f^2} + \Omega t\right) d\Omega \quad (12)$$

known for crystals with single species conductivity [7]. In figure 2, for example, the spectrum of such a pulse covers the whole spectral range of frames (a) and (b). A negative slope of

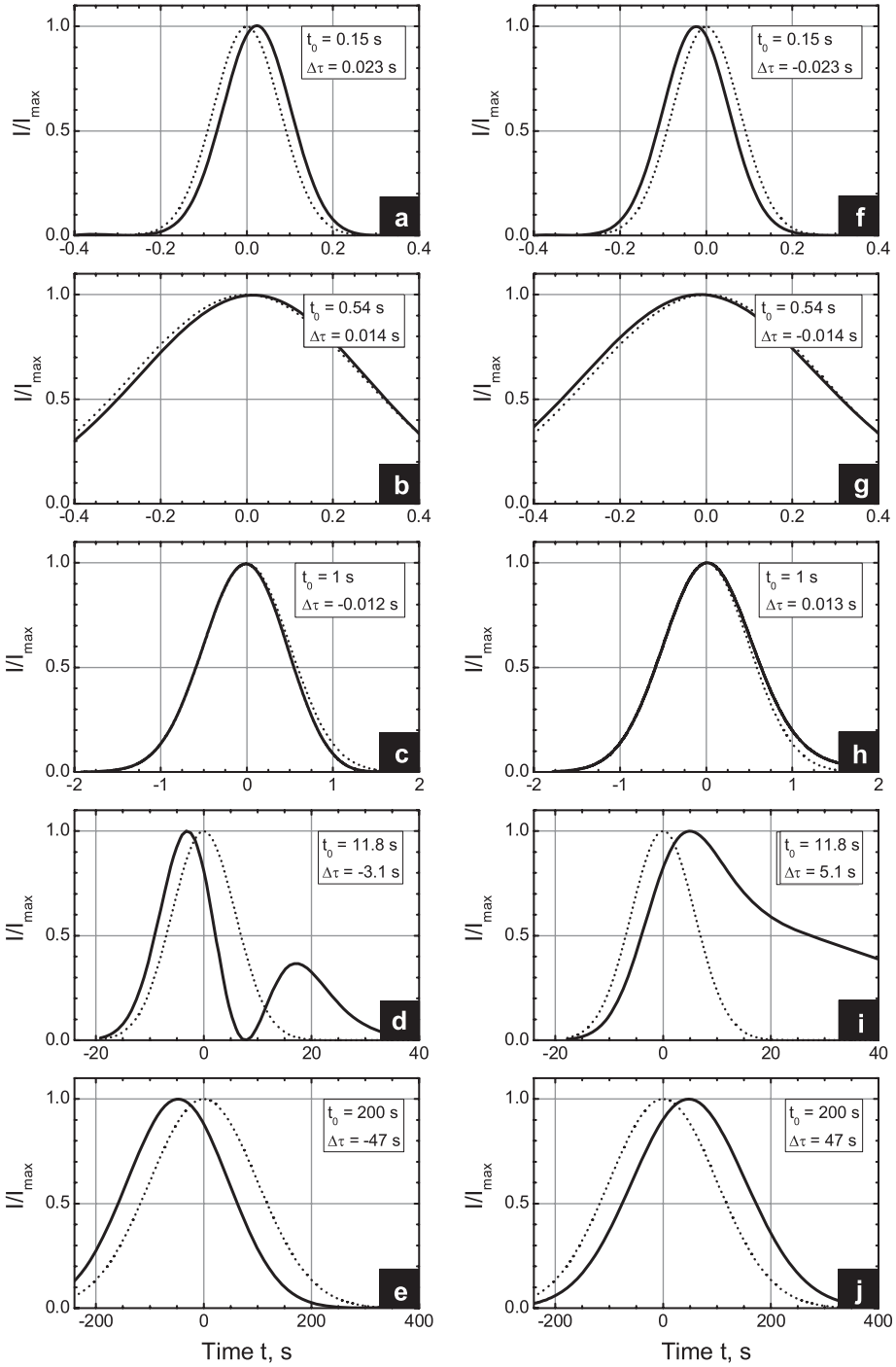


**Figure 6.** Temporal intensity profiles of the input signal pulse (dots) and calculated temporal envelopes at the sample output face (solid lines) for the input pulse durations $t_0 = 0.15$ s, 0.54 s, 1 s, 11.8 s, and 200 s for frames (a) and (f), (b) and (g), (c) and (h), (d) and (i), and (e) and (j), respectively, with $\tau_f = 10$ ms, $\tau_s = 26$ s, $\Gamma_H d = -4$ and $\Gamma_p d = 5$. For the frames from (a) to (e) the orientation of the sample polar axis is chosen to ensure the amplification of the signal pulse, while for frames from (f) to (j) the sample is rotated through 180° and the signal pulse is depleted.

the dependence $\mathrm{Im}\,(\Gamma)d = f(\Omega)$ within the limited range of $\Omega$ is responsible for pulse deceleration and pulse broadening. It should also be recalled that equation (12) describes both the pulse deceleration (or acceleration) and pulse amplification (or depletion, depending on the orientation of the sample polar axis).

The other limit is a very long pulse with $t_0 \gg \tau_s$. In this case the pulse spectrum is very narrow and the condition $\Omega\tau_s \to 0$ holds. The temporal profile of the output pulse is

$$A(d,t) = \frac{A_s(0,t)t_0}{\sqrt{\pi}} \exp\left(\frac{\Gamma_p d}{2}\right) \times \int_0^\infty \exp\left(-\frac{\Omega^2 t_0^2}{4} + \frac{1}{2}\frac{\Gamma_H d}{1+\Omega^2\tau_s^2}\right) \times \cos\left(-\frac{1}{2}\frac{\Omega\tau_s\,\Gamma_H d}{1+\Omega^2\tau_s^2} + \Omega t\right) \mathrm{d}\Omega. \quad (13)$$

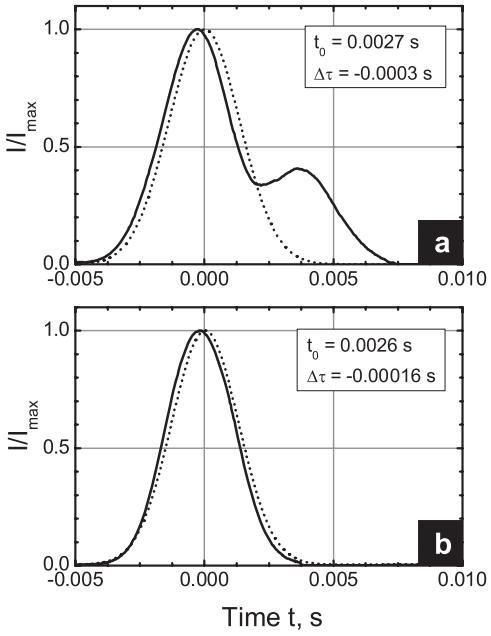


**Figure 7.** Temporal envelopes of the incident pulse (dots) and transmitted pulse (solid line) for the case of pulse amplification: (a) cw pump wave and (b) matched pulses.

Once more, as is evident from equation (13), the solution is reduced to the case of the single species, this time with the characteristic decay time and gain factor of the 'slow' grating under the integral sign. An important distinction of the last equation consists in the additional exponential factor $\exp(\Gamma_p d/2)$ that partially compensates for the decrease (or increase, depending on the orientation of the sample polar axis) of the pulse amplitude that is due to the integral. In such a way the acceleration of the light pulse is achieved with nearly unaffected intensity, as discussed in [23]. In figure 2 this limiting case is illustrated in frames (e) and (f). A positive slope of the dependence $\Im(\Gamma)d = f(\Omega)$ in the vicinity of $\Omega = 0$ ensures pulse advancements which are much larger in absolute value than pulse delays for the short pulses.

The temporal envelopes of the output pulse $|A(d,t)|^2$ shown in figure 6 have been calculated from equation (11) to compare them with those obtained experimentally. The parameters $\tau_f \simeq 10$ ms, $\tau_s \simeq 26$ s, $\Gamma_p d \simeq 5$ and $\Gamma_H d \simeq -4$ were extracted directly from the measured coupling of two cw waves with the same intensities as in the pulse manipulation experiment. The duration of the Gaussian input pulse $t_0$ is 0.15 s, 0.54 s, 1 s, 11.8 s and 200 s for frames (a) and (f), (b) and (g), (c) and (h), (d) and (i), and (e) and (j), respectively; the input beam profile is shown in each frame by a dashed line. The values of $t_0$ in figure 6 correspond exactly to those discussed in the experimental part of this work (see figure 4 for a comparison). A reasonable agreement between the measured data and the results of simulation is obvious.

The processing of the total number of calculated data also allowed for extracting the input-pulse-duration dependences of pulse delay time $\Delta\tau$, pulse duration $W$ and pulse amplification $I_s^{max}(d)/I_s^{max}(0)$. These dependences are shown in figure 5 as solid grey lines together with the experimental data. It should be underlined that this is not a fitting procedure: all parameters such as $\tau_f$, $\tau_s$, $\Gamma_p d$ and $\Gamma_H d$ are taken from an independent experiment on coupling of two cw beams in the same sample. Once more, good agreement of calculation and experiment can be stated.

## 5. Matched pulses

The experimental results and calculations described above show that the acceleration or deceleration of pulses with nearly unaffected pulse shape and best fractional delay or advancement is possible for pulses that meet the requirements (i) $t_0 \geqslant \tau_f$, $t_0 \ll \tau_s$ or (ii) $t_0 \geqslant \tau_f$. For input pulses with the durations that fall within the range between these two time domains the output pulse either acquires a long tail (see figure 6(i)) or becomes split into two consecutive pulses (see figures 6(d) and 4(d)). To minimize the undesirable distortions we use, instead of a cw pump wave, pulsed pump radiation with identical temporal envelopes of the signal and pump pulses. Such a technique is known from pulse deceleration experiments with electromagnetically induced transparency [5], where it is called the matched pulse technique.

The matched pulse technique cannot solve the problem of pulse deterioration completely but it can greatly improve the results obtained. Figure 7 shows a comparison of the experimentally measured temporal envelopes of the accelerated pulses (in geometry with the amplification of the signal beam) for the cw pump and for matched pulses. The input pulse duration $t_0 = 6$ s is roughly half the slow decay time $\tau_s = 10$ s. It is obvious that the pulse twinning which is clearly seen with the cw pump is absent for the case of matched pulses. This improvement is achieved, however, at the expense of more modest advancement time for matched pulses as compared to the cw pump.

The input-pulse-duration dependences of the pulse delay $\Delta\tau$ and pulse duration $W$ are presented in figure 8 for matched signal and pump pulses. They resemble qualitatively those obtained with the cw pump and shown in figures 4(a), (b) and (d). The ultimate measured delays are somewhat smaller with matched pulses but the linearity of the dependence $W = f(t_0)$ becomes better.

## 6. Conclusions

An experimental study of pulse manipulation when writing a dynamic phase grating in $Sn_2P_2S_6$ is described and the results are compared with that calculated within a standard model for a photorefractive crystal with two movable charge carriers in the undepleted pump approximation. Depending on the orientation of the crystal polar axis it is possible to accelerate pulses with duration much shorter than the slow characteristic time of the system and decelerate pulses that are comparable to or longer than this characteristic time, or vice versa.

The main objective of this paper is a demonstration of the principle. The doped $Sn_2P_2S_6$ crystals with higher coupling constants, as described for example in [21], will show similar behaviour with better performance (larger delay times and improved fractional delay). $Sn_2P_2S_6$ crystals can

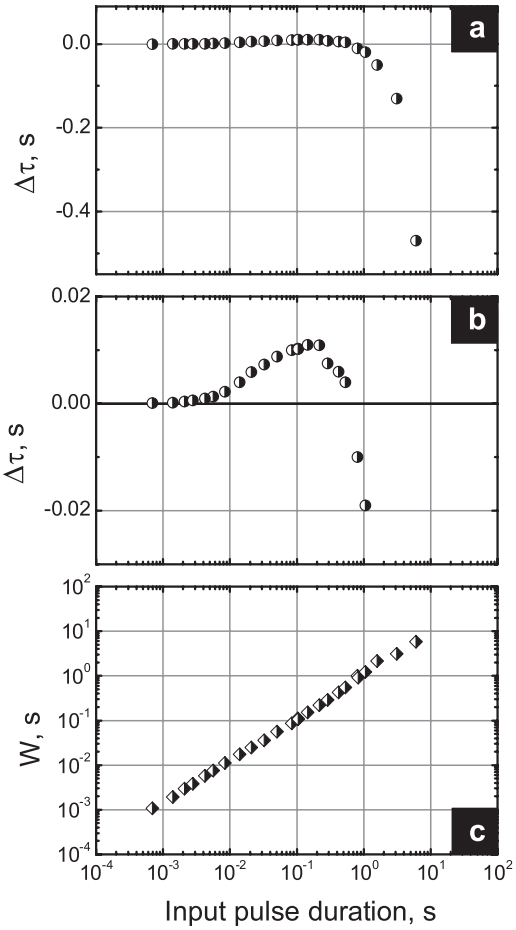


**Figure 8.** Experimentally measured pulse delay time $\Delta\tau$ ((a), (b)) and pulse duration $W$ (c) versus input pulse duration $t_0$ for the case of matched pulses.

offer one more interesting but not yet explored feature: with moderate applied electric field the direction of their polar axis (and thus the direction of the intensity coupling) can be inverted [28]. This opens the possibility of fast switching from pulse acceleration to pulse deceleration by applying short pulses of external electric field.

Other materials than tin hypothiodiphosphate with two out-of-phase gratings can be used for pulse manipulations, too. These are ferroelectric $KNbO_3$ [29], crystals of the sillenite family (BSO [25], BTO [30]) and some photorefractive semiconductors (CdTe:Ge [23], InP:Fe [31]). Usually they all show more modest two-beam coupling gain and therefore should give less effective pulse deceleration or acceleration. For some of them, however, the beam coupling can be greatly improved, for example by using the intensity–temperature resonance in InP:Fe [31] or profiting from the Franz–Keldysh effect near the band edge [32]. This allows us to expect at least comparable performance with these materials as with $Sn_2P_2S_6$.

## Acknowledgments

The authors are grateful to A Grabar and I Stoyka (Institute of Solid State Physics and Chemistry, Uzhgorod National University, Ukraine) for $Sn_2P_2S_6$ samples.

## References

[1] Brillouin L 1960 *Wave Propagation and Group Velocity* (New York: Academic)
Sommerfeld A 1914 *Ann. Phys. Lpz* **44** 177
Brillouin L 1914 *Ann. Phys. Lpz* **44** 203
[2] Masumoto Y, Unuma Y, Tanaka Y and Shionoya S 1979 Picosecond time of flight measurements of excitonic polariton in CuCl *J. Phys. Soc. Japan* **47** 1844–9
[3] Scheuer J, Paloczi J T, Poon Joyce K S and Yariv A 2005 Coupled resonator optical waveguides: toward the slowing and storage of light *Opt. Photon. News* **16** 36–40
[4] Lin S, Hsu K and Yeh P 2000 Experimental observation of the slowdown of optical beams by a volume-index grating in a photorefractive $LiNbO_3$ crystal *Opt. Lett.* **25** 1582–4
[5] Hau L V, Harris S E, Dutton Z and Behroozi C 1999 Light speed reduction to 17 m $s^{-1}$ in an ultracold atomicgas *Nature* **397** 594–8
Harris S 1997 Electromagnetically induced transparency *Phys. Today* **50** 36–42
[6] Boyd R W and Gauthier D J 2002 'Slow' and 'fast' light *Prog. Opt.* **43** 497–530
[7] Podivilov E, Sturman B, Shumelyuk A and Odoulov S 2003 Light pulse slowing down up to 0.025 cm $s^{-1}$ by photorefractive two-wave coupling *Phys. Rev. Lett.* **91** 083902
[8] Deng Zh and Hemmer Ph R 2003 Investigation of room-temperature slow light in photorefractives for optical buffer applications *Proc. SPIE* **5362** 81–9
[9] Zhang G, Dong R, Bo F and Xu J 2004 Slowdown of group velocity of light by means of phase coupling in photorefractive two-wave mixing *Appl. Opt.* **43** 1167–73
Zhang G, Bo F, Dong R and Xu J 2004 Phase-coupling-induced ultraslow light propagation in solids at room temperature *Phys. Rev. Lett.* **93** 133903
[10] Deng Z, Quiing D-K, Hemmer P R, Raymond Ooi, Zubairy M S and Scully M O 2006 Time-bandwidth problem in room temperature slow light *Phys. Rev. Lett.* **96** 023602
[11] Yum H N, Salit M, Pati G S, Tseng S, Hemmer P R and Shahriar M S 2008 Fast-light in a photorefractive crystal for gravitational wave detection *Opt. Express* **16** 20448–56
[12] Shumelyuk A M, Hryhorashchuk A I and Odoulov S G 2009 Optical forerunners in crystals with photorefractive dynamic gratings *Ukr. J. Phys.* **54** 33–7 http://ujp.bitp.kiev.ua/files/file/papers/54/1-2/540106p.pdf
[13] Zhang G, Bo F and Xu J 2007 Slow and fast lights in photorefractive materials *Photorefractive Materials and Their Applications 3,* ed P Günter and J-P Huignard (New York: Springer) pp 277–93
[14] von Bassevitz J, Horn W and Denz C 2009 Slow and fast light in photorefractive SBN:60 using contra-directional mixing geometry *PR'09: Proc. Topical Mtg Photorefractive Materials, Effects, and Devices. Control of Light and Matter (Bad Honef)* pp 252–3
[15] Sturman B I, Podivilov E V and Gorkunov M V 2008 Photorefractive manipulation of light pulses *Phys. Rev.* A **77** 063808
[16] Sturman B, Mathey P, Rebhi R and Jauslin H 2009 Nonlinear pulse deceleration using photorefractive four-wave mixing *J. Opt. Soc. Am.* B **26** 1949–53
Sturman B, Podivilov E and Gorkunov M 2009 Deceleration and shape-transformation of light pulses during phase conjugation in photorefractive media *Appl. Phys.* B **95** 545–9
[17] Odoulov S, Shumelyuk A, Hellwig U, Rupp R, Grabar A and Stoyka I 1996 Photorefraction in tin hypothiodiphosphate in the near infrared *J. Opt. Soc. Am.* B **13** 2352–60
[18] Grabar A, Jazbinšek M, Shumelyuk A, Vysochanskii Yu M, Momtemezzani G and Günter P 2007 Photorefractive effects

in $Sn_2P_2S_6$ *Photorefractive Materials and Their Applications 3,* ed P Günter and J-P Huignard (New York: Springer) pp 327–62

[19] Mosimann R, Marty P, Bach T, Juvalta F, Jazbinsek M, Günter P and Grabar A A 2007 High-speed photorefraction at telecommunication wavelength 1.55 $\mu$m in $Sn_2P_2S_6$:Te *Opt. Lett.* **32** 3230–2

[20] Kedyk I V, Mathey P, Gadret G, Bidault O, Grabar A A, Stoyka I M and Vysochanskii Yu M 2008 Enhanced photorefractive properties of Bi-doped $Sn_2P_2S_6$ *J. Opt. Soc. Am.* B **25** 180–6

[21] Bach T, Jazbinsek M, Momtemezzani G, Günter P, Grabar A A and Vysochanskii Yu M 2007 Tailoring of infrared photorefractive properties of $Sn_2P_2S_6$ crystals by Te and Sb doping *J. Opt. Soc. Am.* B **24** 1535–41

[22] Shumelyuk A, Odoulov S and Brost G 1999 Multiline coherent oscillation in photorefractive crystals with two species of movable carriers *Appl. Phys.* B **68** 959–66

[23] Shumelyuk A, Shcherbin K, Odoulov S, Sturman B, Podivilov P and Buse K 2004 Slowing down of light in photorefractive crystals with beam intensity coupling reduced to zero *Phys. Rev. Lett.* **93** 243604

[24] Haertle D, Caimi G, Haldi A, Montemezzani G, Günter P, Grabar A A, Stoika I M and Vysochanskii Yu M 2003 Electro-optical properties of $Sn_2P_2S_6$ *Opt. Commun.* **215** 333–43

[25] Zhivkova S and Miteva M 1990 Holographic recording in photorefractive crystals with simultaneous electron–hole transport and two active centers *J. Appl. Phys.* **68** 3099–103

[26] Frejlich J 2006 *Photorefractive Materials: Fundamental Concepts, Holographic Recording, and Materials Characterization* (New York: Wiley–Interscience)

[27] Sturman B, Mathey P, Jauslin H R, Odoulov S and Shumelyuk A 2007 Modeling of the photorefractive nonlinear response in $Sn_2P_2S_6$ crystals *J. Opt. Soc. Am.* B **24** 1303–9

[28] Shumelyuk A, Odoulov S, Kip D and Krätzig E 2001 Electric-field enhancement of beam coupling in $Sn_2P_2S_6$ *Appl. Phys.* B **72** 707–10

[29] Montemezzani G, Zgonik M and Günter P 1993 Photorefractive charge compensation at elevated temperatures and application to $KNbO_3$ *J. Opt. Soc. Am.* B **10** 171–85

[30] Donnermeyer A, Vogt H and Krätzig E 2003 Complimentary gratings due to electron and hole conductivity in aluminium-doped bismuth titanium oxide crystals *Phys. Status Solidi* a **200** 451–6

[31] Abdelghani-Idrissi A, Ozkul C, Wolffer N, Gravey P and Piccoli G 1991 Resonant behaviour of the temporal response of the two-wave mixing in photorefractive InP:Fe crystals under dc fields *Opt. Commun.* **86** 317–23

[32] Partovi A, Kost A, Garmire E M, Valley G C and Klein M B 1990 Band-edge photorefractive effect in semiconductors *Appl. Phys. Lett.* **56** 1089–91